Proton-Deuteron Elastic Triple Scattering at 140 MeV*

R. A. HOFFMAN,† J. LEFRANÇOIS,‡ AND E. H. THORNDIKE§
Cyclotron Laboratory, Harvard University, Cambridge, Massachusetts
(Received 27 March 1963)

Measurements of the proton-deuteron elastic triple scattering parameters R and A have been made at the indicated laboratory energies. The following results were obtained:

θ_{lab}	R(140 MeV)	A(137½ MeV)
20°	0.404±0.101	−0.377±0.099
25°	0.180±0.105	−0.301±0.082
30°	0.064±0.085	−0.038±0.075
35°	−0.096±0.092	+0.191±0.074
40°	0.153±0.156	···

Formulas, based on the impulse approximation, are given relating various elastic scattering parameters to nucleon-nucleon scattering amplitudes. The expressions were evaluated using nucleon-nucleon amplitudes of Breit and collaborators, and of Gammel and Thaler, and were compared with the R and A measurements, and with cross-section and polarization measurements of Postma and Wilson. The fit for solutions YLAN 3 and 3M is adequate for angles less than 45° lab.

I. INTRODUCTION

PROTON-DEUTERON inelastic scattering is discussed experimentally in the preceding paper,[1] and theoretically in the following paper.[2] This article is devoted to elastic scattering. Measurements of the differential cross section and polarization for elastic scattering have been made at 147 MeV[3], and at other energies. (A summary of these other measurements is given by Postma and Wilson.[3]) Here, we report measurements of the triple scattering parameters R at 140 MeV and A at 137½ MeV, and compare these measurements and the cross-section and polarization measurements of Postma and Wilson with the theoretical predictions of the impulse approximation.

The primary experimental problem which differentiates these experiments from, say, proton-proton triple scattering experiments,[4] is that of separating the desired elastic events from the unwanted inelastic events. Elastically scattered protons are characterized by their higher and unique energy, and by the accompanying recoil deuterons. For the angular range under consideration here (20° to 40° lab), the recoil deuterons have low energy and do not all escape from the target. For this reason, and for reasons of simplicity, no attempt was made to detect the recoil deuterons; elastic events were identified on the basis of energy alone. Because of the poor energy resolution of this experiment, the separation of elastic and inelastic events was not clean; a sizeable number of inelastically scattered protons fell under the elastic peak. The number of such events was estimated from cross-section considerations; the values of R and A for such events were calculated from theory. In this way, a correction was made for the inelastic contamination.

In the next section (Sec. II), the experimental method is discussed. In Sec. III, the problem of correcting for inelastic contamination is discussed. The values of R and A, with their errors, are presented in Sec. IV. An impulse-approximation analysis of these results, along with the cross-section and polarization measurements of Postma and Wilson,[3] is given in Sec. V. Section VI contains a summary and conclusion.

II. EXPERIMENTAL METHOD

1. General

The p-d elastic scattering measurements were carried out simultaneously with the p-d inelastic scattering measurements described in I. The experimental layout and a block diagram of the electronic circuitry are shown in Figs. 1 and 2 of that article. The reader is referred there for a description of most aspects of the procedure. The experiments differed primarily in the method of identifying the desired events. Thus, quasifree p-p events were identified by detecting a recoil proton in counter P in time coincidence with counters B, C, D or B, E, F. Quasifree p-n events were identified by detecting a recoil neutron in counter N in coincidence with counters B, C, D or B, E, F. The method of identification of elastic scattering events is described in the next paragraphs.

For the elastic scattering experiment, counters P, N,

* Supported by the joint program of the U. S. Office of Naval Research and the U. S. Atomic Energy Commission.
† Present address: The Department of Physics, Union College, Schenectady, New York.
‡ Present address: The Laboratoire des Hautes Energies, Orsay, France.
§ Present address: The Department of Physics, University of Rochester, Rochester, New York.
[1] J. Lefrançois, R. A. Hoffman, E. H. Thorndike, and Richard Wilson, preceding paper, Phys. Rev. **131**, 1660 (1963), hereafter referred to as I.
[2] A. H. Cromer and E. H. Thorndike, following paper, Phys. Rev. **131**, 1680 (1963), hereafter referred to as III.
[3] H. Postma and Richard Wilson, Phys. Rev. **121**, 1229 (1961), and private communications.
[4] E. H. Thorndike, J. Lefrançois, and Richard Wilson, Phys. Rev. **120**, 1819 (1960).

C, and D were not used. Only the circuitry shown in the left-hand third of the block diagram (I, Fig. 2) was used. The incident beam, after passing through the magnets (R) and (M), the defining slits (H), and ion chamber (S), struck the liquid-deuterium target (2). Protons scattered through an angle θ_2 passed through counter B and struck the third scatterer (3). Protons scattering in the vertical plane here at an angle θ_3 passed through counter E, some absorbers (K), counter F, more absorbers (K), and entered counter G, a total energy counter 8 in.$\times 3\frac{1}{2}$ in.$\times 2$ in. thick. The thicknesses of the various absorbers were such as to prevent some inelastically scattered protons from entering G, and to insure that all elastically scattered protons stopped somewhere in the G counter.

2. Electronic Circuitry

The outputs of counters B, E, and F went to a coincidence circuit. The output of counter G went to a linear gate.[5] The gate was opened by a BEF coincidence. The output of the gate was stretched and amplified, and then sent both to a variable discriminator and scaler and to a 100-channel pulse-height analyzer (P.H.A.). The discriminator setting could be related to the P.H.A. scale, i.e., all pulses above the discriminator setting were also above a readily determined channel in the P.H.A. This channel is referred to as the "cutting point." Those pulses above the discriminator setting (and thus counted by the scaler) are referred to as "BEFG coincidences."

When only triply scattered protons could be detected by the EFG telescope (i.e., $\theta_3 = 15°$), the counting rates were low enough so that dead time losses in the P.H.A. and in the BEFG coincidence circuitry were both negligible. However, when doubly scattered protons could enter the EFG telescope (i.e., $\theta_3 < 10°$), dead time losses were large. BEFG losses could be reduced to negligible proportions by inserting a fast scale-of-4 between the output of the BEF coincidence circuit and the gating input. P.H.A. losses could be reduced to tolerable proportions only by reducing the incident beam intensity.

3. Procedure

The beam, target, and scattering table were aligned as described in I. The absorber between counters E and F was set as dictated by that experiment.

The angle θ_3 was set at zero, the incident-beam intensity was reduced, and P.H.A. spectra were taken. The amount of absorber between F and G was varied to ascertain that all elastically scattered protons were stopped in counter G. There was substantial latitude in the choice of this absorber. Typical P.H.A. spectra are shown in Figs. 1 and 2. In Fig. 1, the absorber between F and G was chosen to allow a large part of the inelastically scattered protons to enter the G counter; in Fig. 2, it was chosen to allow a much smaller number of inelastically scattered protons to enter G. It was initially hoped that the spectrum of inelastically scattered protons (as in Fig. 1) could be extrapolated under the elastic peak, to give the amount of inelastic contamination. This did not prove feasible (see Sec. III), and so during the later runs, the absorber was chosen to give spectra more like Fig. 2. Such spectra were less sensitive to changes in gain in the electronic circuitry (see Sec. II. 4 data reduction).

The cutting point was chosen; it is indicated for typical cases in Figs. 1 and 2. The choice is a compromise between the desire to exclude as many inelastic events

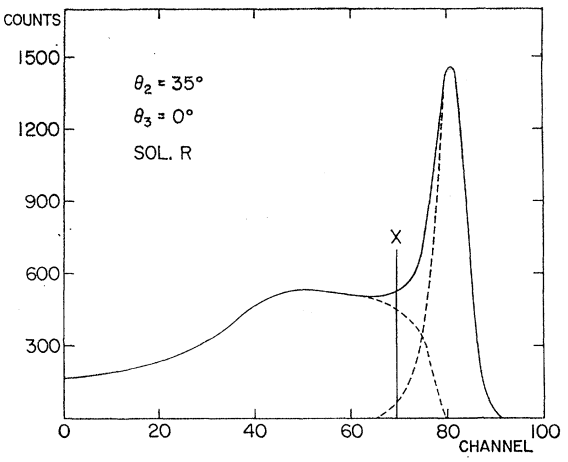

FIG. 1. Typical P.H.A. spectrum of the doubly scattered beam ($\theta_3 = 0$), containing a large part of the inelastically scattered protons, in addition to the elastic peak. The dashed curves show the separation into elastic and inelastic scattering, by the method described in Section III 2. The cutting point X is shown.

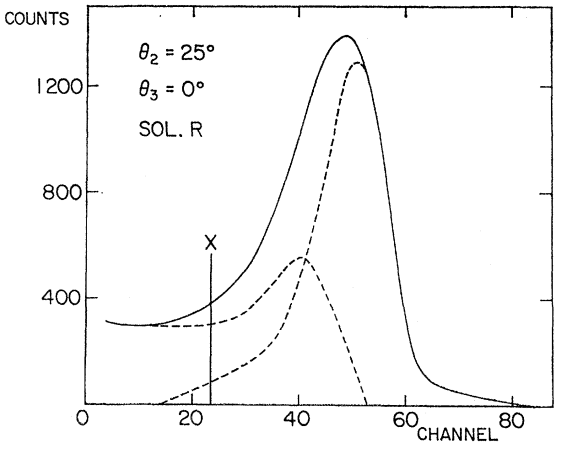

FIG. 2. Typical P.H.A. spectrum of the doubly scattered beam ($\theta_3 = 0$), containing a small fraction of the inelastically scattered protons, in addition to the elastic peak. The dashed curves show the separation into elastic and inelastic scattering, by the method described in Sec. III 2. The cutting point X is shown.

[5] This transistorized circuit had a gating time of 0.1 μsec, and was linear to 2% for input signals from 0.8 to 8 V. It is described by Lefrançois, thesis, Harvard University, 1961 (unpublished).

as possible (by moving the cutting point up) and the desire to have a situation stable against small gain changes (by moving the cutting point down: see discussion in Sec. II. 4).

The $\theta_3=0°$ misalignment was measured as described in I. The incident beam was at full intensity; the prescaler was in the BEF coincidence output. BEFG coincidences were used; the P.H.A. was not. For this purpose it was felt that BEFG coincidences would give an adequate measure of the misalignment of the *p-d* elastic events. (Misalignments measured for BEF and BEFG differed only slightly, indicating that the amount of inelastic contamination did not affect the misalignment much.)

The asymmetry was measured as described in I. The direction of polarization of the incident beam was reversed at about 30-min intervals. The sense of the third scattering angle θ_3 was reversed at about 6-h intervals. Each time the angle θ_3 was to be reversed, the EFG telescope was fixed at $\theta_3=0°$, the incident-beam intensity was reduced, and P.H.A. spectra were taken, usually for both solenoid directions. In this way gain drifts were monitored.

Background from the target cup and other material near the target was measured, following the same procedure as for the asymmetry measurement, after evacuating the target. Additional copper absorber was placed between E and F to compensate for the change in energy of the scattered particles due to the absence of deuterium in the target. The background rate was typically 4% of the "target full" rate.

Random coincidences between B and EFG were measured periodically during the asymmetry measurement. This random rate was 0.5%, or less, of the total counting rate. Random coincidences between BEF and G were not measured routinely. They were shown to be less than 0.3% of the total counting rate, and thus could be ignored.

4. Data Reduction

On the basis of the spectra measured at $\theta_3=0°$ every 6 h during data collection, some of the asymmetry data were discarded. Data were kept for analysis only if the gain monitoring spectra indicated a stability of 2% or better. The asymmetry data from the pulse-height analyzer were added channel by channel to form four final spectra: EF up, solenoid normal; EF up, solenoid reversed; EF down, solenoid normal; EF down, solenoid reversed. A typical final spectrum is shown in Fig. 3.

If the choice of cutting point made during the run seemed poor, a new cutting point was chosen. All counts above the cutting point were summed, and used to calculate the asymmetry.

This asymmetry was corrected for random coincidences between B and EFG, target empty background, and the θ_3 misalignment. For this last correction, the value of the slope $(1/\sigma)(d\sigma/d\theta)$ was interpolated from the data of Thorndike *et al.*[4] measured with the same scattering table. For the R measurements, a correction to the asymmetry due to the energy variation of the incident beam at the defining slits was applied, as described in I. For the A measurement, this correction was zero.

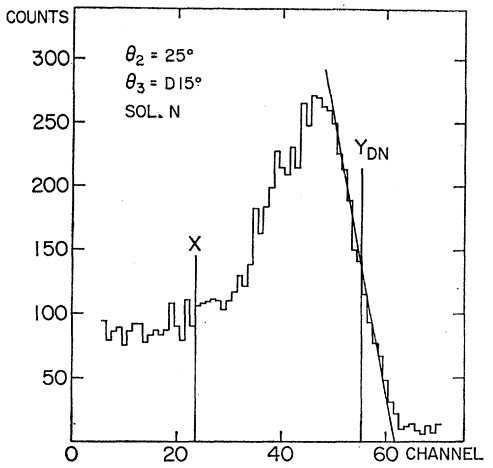

FIG. 3. Typical P.H.A. spectrum of the triply scattered beam ($\theta_3=15°$), showing the cutting point X, and the upper half-way-down point Y.

The asymmetries, corrected as indicated above, are shown in Table I. Each error listed is a quadratic combination of: errors from counting statistics in the raw data, the background, and the random coincidences; the error in the misalignment correction; and the error in the slit energy variation correction.

Small long-term drifts in the incident-beam energy, or in the gain of the G counter and following circuitry (roughly 2% per day) were observed in the gain monitoring spectra. To first order, these drifts caused no error in the asymmetry, since the solenoid was reversed every 30 min. Systematic changes with solenoid current direction or EFG telescope position would have been more serious, and might have caused false asymmetries. Such changes could be caused by a change in incident-beam energy with solenoid current direction or by changes in phototube gain due to magnetic-field variations either with G counter position or solenoid current direction.

A correction was made for possible gain shifts as follows: On each of the four final spectra, the point, in

TABLE I. Asymmetries as calculated from the pulse-height analyzer spectra. The listed asymmetries are corrected for background, misalignments, etc. (see text), but not for shifts in gain. This correction $\delta\epsilon$ is listed separately.

	R Measurement		A Measurement	
θ_2(lab)	Asymmetry ϵ	Gain-shift correction $\delta\epsilon$	Asymmetry ϵ	Gain-shift correction $\delta\epsilon$
20°	$+0.055\pm0.006$	-0.007 ± 0.008	$+0.078\pm0.007$	-0.002 ± 0.010
25°	$+0.021\pm0.007$	-0.004 ± 0.013	$+0.059\pm0.005$	-0.001 ± 0.006
30°	$+0.001\pm0.007$	-0.001 ± 0.005	$+0.007\pm0.008$	$+0.001\pm0.008$
35°	-0.023 ± 0.010	$+0.001\pm0.010$	-0.029 ± 0.009	-0.001 ± 0.003
40°	$+0.005\pm0.012$	$+0.016\pm0.017$	...	...

the upper part of the spectrum, where the counting rate per channel had dropped to one-half of its peak value, was located. This "upper half-way-down" point Y could be located to within $\pm\frac{1}{2}$ to ± 1 channel, depending on the sharpness of the elastic peak. The upper half-way-down point for a typical spectrum is indicated in Fig. 3. The false asymmetry is given by

$$\delta\epsilon = C\frac{N}{N_T}(Y_{DN}+Y_{UR}-Y_{UN}-Y_{DR}). \quad (1)$$

N_T is the total number of events with pulse height higher than the cutting point. N is the number of counts in the channel adjacent to the cutting point. C is a constant which takes into account the fact that a shift in gain corresponds to a shift of a different number of channels at the cutting point than at the upper half-way-down point. If the shifts in Y are due purely to electronic circuitry changes, then C should be smaller than one; if the shifts are due purely to beam energy changes, then C should be larger than one. We have used $C=1$, and included as an error differences in the corrections corresponding to extreme possible values of C.

The correction to the asymmetry from the shift in half-way-down point, and the error in this correction are listed in Table I. Each error includes the uncertainty in determining the half-way-down points, and the uncertainty in the value of C. The former is dominant. From Table I, one can see that the error on the correction is comparable to the error on the asymmetry. Thus, minimizing the error on the correction is important. This can be accomplished by moving the cutting point to lower channels, reducing the ratio N/N_T of Eq. (1). However, moving the cutting point down increases the error from inelastic contamination, as discussed in Sec. III. Increasing the amount of absorber between F and G reduces the false asymmetry caused by electronic drifts, but increases the false asymmetry caused by shifts in the incident-beam energy.

III. INELASTIC CONTAMINATION

1. General

The value of the asymmetry for events above the cutting point is

$$\epsilon = f\epsilon_{pd}+(1-f)\epsilon_{\text{in}}, \quad (2)$$

where f is the fraction of the events above the cutting point which consist of p-d elastic scattering events, ϵ_{pd} is the asymmetry of elastic events, and ϵ_{in} is the asymmetry of inelastic events above the cutting point. For the R measurement, Eq. (2) can be solved to give

$$R_{pd}=\frac{\epsilon}{fP_1P_{3\,\text{el}}}-R_{\text{in}}\left(\frac{P_1P_{3\,\text{in}}}{P_1P_{3\,\text{el}}}\right)\left(\frac{1-f}{f}\right). \quad (3)$$

A similar expression exists for A.

Section II was devoted primarily to the determination of ϵ. In this section, we discuss the other quantities on the right-hand side of Eq. (3).

2. Determination of f

The value of f was determined by analysis of the P.H.A. spectra taken with doubly scattered protons ($\theta_3=0°$). The percentage contamination $(1-f)/f$ will be slightly different for triply scattered protons ($\theta_3=15°$); since inelastically scattered protons have a lower energy at the third scatterer, they will have a higher cross section and, hence, be favored. This effect decreases f by $(2\pm 1.5)\%$.

Postma and Wilson[3] for their cross-section and polarization measurements determined f and the error on f by extrapolating the inelastic part of the spectrum under the elastic peak. From the most probable extension, they calculated the value of f; the error on f was obtained from the difference in values of f from extreme extensions. Because of the poor energy resolution of our experiment, this method would give a 30% uncertainty in f.

It was, thus, decided to determine f from absolute cross-section considerations, using Postma and Wilson's values of cross sections.[3] N, the number of events above the cutting point per beam monitor unit, is given by

$$N=K(\alpha\sigma_{pd}+X). \quad (4)$$

K is a normalizing constant, including target thickness, solid angle, incident protons per beam monitor unit, etc. X is an effective inelastic cross section, which is not needed to obtain f. α is that fraction of the elastic events which lie above the cutting point; it was always greater than 0.9. In terms of Eq. (4),

$$f=\frac{K\alpha\sigma_{pd}}{N}. \quad (5)$$

An iterative procedure was used to obtain f. A trial value of α was assumed and f calculated from Eq. (5). The inelastic and elastic contributions to the spectrum were separated, such that they would give the right value of f. This separation was essentially unique if a reasonably symmetric shape was assumed for the

TABLE II. Contamination of the p-d elastic R data from inelastic events.

θ_2(lab)	f^{*}[a]	f_s	f_t	f_{pp}	f_{pn}	ΔE^{**}[b] (MeV)	f^t[c]
20°	0.62±0.06	0.34	0.21	0.23	0.22	8.7	0.60±0.04
25°	0.65±0.06	0.34	0.39	0.15	0.12	8.7	0.60±0.04
30°	0.69±0.07	0.38	0.55	0.04	0.03	6.3	0.73±0.05
35°	0.84±0.08	0.39	0.60	0.006	0.004	4.5	0.85±0.05
40°	0.82±0.08	0.27	0.70	0.02	0.01	4.8	0.85±0.05

[a] f^{*}, value of f calculated by Eq. (5) of text; error = 10% of f^{*}.
[b] ΔE^{**}, (energy of elastic events) − (cutting point energy).
[c] f^t, value of f calculated by Eq. (9) of text; error from 1-MeV uncertainty in cutting-point energy.

elastic peak. A new value of α was obtained from the separated elastic spectrum, and the whole procedure repeated, if necessary, until it converged. Typical elastic and inelastic separations are shown in Figs. 1 and 2. Values of f obtained in this way are listed in Tables II and III.

3. Determination of R_{in} and A_{in}

This section will be written in terms of determining R_{in}. To have it explain the determination of A_{in}, merely replace R by A wherever it appears.

The value of R_{in} was determined from a theoretical treatment of Cromer.[6] He calculates in impulse approximation, and includes the s-wave part of the final-state interaction between the target particles. He finally writes, for inelastic scattering:

$$\frac{d^2\sigma}{d\Omega_2 dE_2}(E_2)=\frac{\alpha(E_2)}{3}\Sigma_s+\beta(E_2)\Sigma_t+\gamma(E_2)(\sigma_{np}+\sigma_{pp}) \quad (6)$$

and

$$\frac{d^2\sigma}{d\Omega_2 dE_2}(E_2)R(E_2)=\frac{\alpha(E_2)}{3}\Sigma_s R_s+\beta(E_2)\Sigma_t R_t +\gamma(E_2)(\sigma_{np}R_{np}+\sigma_{pp}R_{pp}). \quad (7)$$

E_2 is the energy of the inelastically scattered proton. $\alpha(E_2)$, $\beta(E_2)$, and $\gamma(E_2)$ are "form-factor-like" quantities which come from the calculations. σ_{np} and σ_{pp} are the n-p and p-p cross sections, while R_{np} and R_{pp} are the n-p and p-p R parameters. Σ_t and Σ_s are related to the cross sections for scattering leaving the target particles in a triplet- or singlet-spin state, respectively; R_t and R_s are the R parameters for scattering to these states. Formulas relating Σ_t, R_t, and A_t to nucleon-nucleon amplitudes are given in Table VIII, Sec. V, while formulas for Σ_s, R_s, and A_s appear in III. To the extent that the impulse approximation is valid for p-d elastic scattering, $R_{pd}=R_t$, $A_{pd}=A_t$, and $\sigma_{pd}=\Sigma_t F^2(q)$, where $F(q)$ is the deuteron form factor.

TABLE III. Contamination of the p-d elastic A data from inelastic events.

θ_2(lab)	f^{*a}	f_s	f_t	f_{pp}	f_{pn}	ΔE^{**b} (MeV)	$f^{t\,c}$
20°	0.68±0.07	0.48	0.31	0.11	0.10	5.6	0.66±0.08
25°	0.63±0.06	0.41	0.43	0.09	0.07	6.0	0.62±0.09
30°	0.69±0.07	0.40	0.54	0.04	0.02	6.0	0.76±0.10
35°	0.82±0.08	0.35	0.61	0.03	0.01	3.9	0.74±0.07

[a] f^*, value of f calculated by Eq. (5) of text; error = 10% of f^*.
[b] ΔE^{**}, (energy of elastic events) − (cutting point energy).
[c] f^t, value of f calculated by Eq. (9) of text; error from 1-MeV uncertainty in cutting-point energy.

[6] A. H. Cromer, Phys. Rev. **129**, 1680 (1963), and private communications.

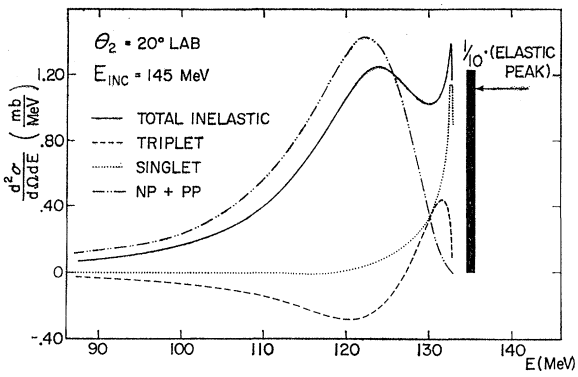

FIG. 4. Inelastic cross section versus energy of the inelastically scattered proton, according to the theoretical treatment of Cromer, Ref. 6. See text for fuller explanation of the various curves. The elastic peak, spread over 1 MeV and reduced by a factor of 10, is shown for comparison.

The three terms on the right of Eq. (6), plus their sum, the total inelastic cross section, are plotted for two scattering angles in Figs. 4 and 5. The elastic peak, spread over 1 MeV, is shown for comparison. Only the upper 5 to 10 MeV of the inelastic spectra are above the cutting point. At $\theta_2=20°$, singlet scattering is dominant, though all types of scattering are important. At $\theta_2=35°$, triplet scattering is dominant, and $np+pp$ scattering has become negligible, since it is well separated in energy from the elastic peak.

We integrate each of the terms in Eqs. (6) and (7) over E_2, from the maximum energy for inelastic events to the energy corresponding to the cutting point. This threshold energy can be calculated to ±1 MeV, and is given in Tables II and III. From the integrated values of $\frac{1}{3}\alpha\Sigma_s$, $\beta\Sigma_t$, $\gamma\sigma_{np}$, and $\gamma\sigma_{pp}$, we calculated the fraction of the inelastic contamination caused by singlet type of events, triplet events, etc. These fractions are denoted f_s, f_t, f_{pp}, and f_{np}, and are listed in Tables II and III. Experimental values of σ_{pp}, σ_{np}, and $\Sigma_t=\sigma_{pd}/F^2(q)$ were

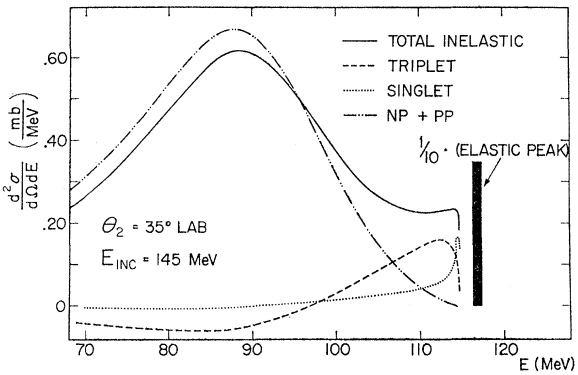

FIG. 5. Inelastic cross section versus energy of the inelastically scattered proton, according to the theoretical treatment of Cromer, Ref. 6. See text for fuller explanation of the various curves. The elastic peak, spread over 1 MeV and reduced by a factor of 10, is shown for comparison.

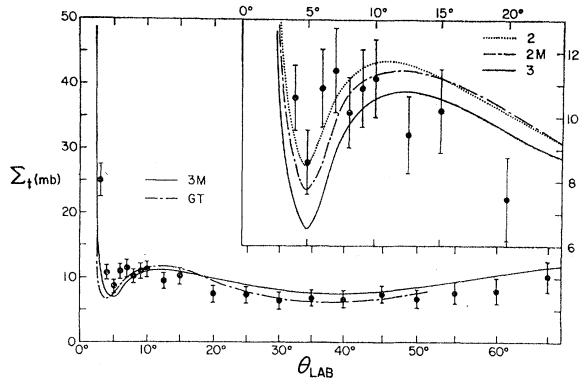

FIG. 6. Cross-section parameter Σ_t versus laboratory scattering angle; the experimental points come from the cross-section measurements of Ref. 3, and the form-factor measurements of Ref. 8. The curves are evaluations of the expression for Σ_t given in Table VIII using the nucleon-nucleon amplitudes of Ref. 9 (YLAN 2, 2M, 3, 3M) and Ref. 11 (GT).

used.[3,7,8] Σ_s was calculated from the formula of Table VIII of III, using nucleon-nucleon amplitudes from the n-p phase-shift solution YLAN-3M and p-p solution YLAM, of Breit and collaborators.[9]

From Eqs. (6) and (7) and the definitions of f_s, f_t, etc.,

$$R_{\text{in}}=\frac{f_sR_s+f_tR_t+f_{pp}R_{pp}+f_{np}R_{np}}{f_s+f_t+f_{pp}+f_{np}}, \qquad (8)$$

with, of course, a similar expression holding for A_{in}. R_{pp} and A_{pp} were taken from the free proton-proton experiments at 140 MeV.[4,10] R_{np} and A_{np} were taken from the quasifree p-n experiments (see I), after corrections to relate these to free n-p scattering had been applied. Errors of ±0.05 were added to the experimental errors on R_{pp}, A_{pp}, R_{np}, and A_{np} to allow for off-energy-shell effects. R_t was taken as R_{pd}, and A_t was taken as A_{pd}. Errors of ±0.05 were attached to the measured values to take into account possible differences between R_{pd} and R_t and A_{pd} and A_t. The normal experimental errors on R_{pd} and A_{pd} were not included, as these cancel when Eq. (8) is inserted into Eq. (3). R_s and A_s were calculated from the formulas of Table VIII of III, using amplitudes from solutions YLAN-3M, and YLAM[9]. Calculations were also done using other Yale n-p amplitudes[9] besides 3M, and using Gammel-Thaler n-p and p-p amplitudes.[11] Results are shown in Figs. 6 and 7 of III. Note the small differences between the curves for A_s, and the large differences between the curves for R_s. The error attached to A_s was ±0.2, while the error attached to R_s was ±0.2 or $\frac{1}{2}$ the extreme difference between the various curves of Fig. 6, whichever was larger. An error of 10% of their values was attached to f_{pp}, f_{pn}, and f_t. The error on f_s ranged from 15% at 20° to 35% at 40°. The values of R_{in} and A_{in} are given in Table IV.

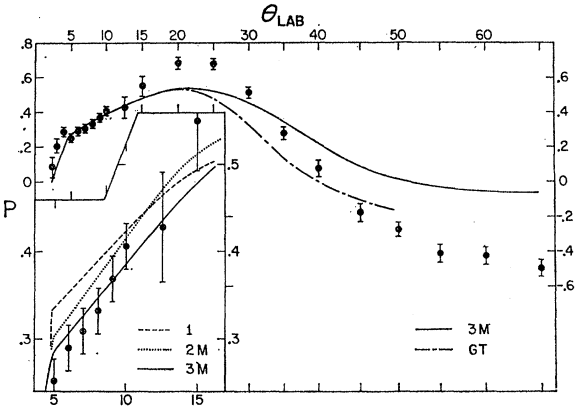

FIG. 7. Polarization versus laboratory scattering angle. The experimental points come from measurements of Ref. 3. The curves are evaluations of the expression for P given in Table VIII using the nucleon-nucleon amplitudes of Ref. 9 (YLAN 1, 2M, 3M) and Ref. 11 (GT).

TABLE IV. Values of R_{in} and A_{in}.

θ_2(lab)	R_{in}	A_{in}
20°	-0.18 ± 0.09	-0.12 ± 0.10
25°	-0.16 ± 0.09	-0.14 ± 0.09
30°	-0.15 ± 0.15	-0.04 ± 0.09
35°	-0.20 ± 0.15	$+0.08\pm0.08$
40°	-0.01 ± 0.10	...

Equation (6) provides an alternative method of obtaining the quantity f. In particular,

$$\frac{1-f}{f}=\frac{1}{\sigma_{pd}}\int\frac{d^2\sigma}{d\Omega_2 dE_2}dE_2, \qquad (9)$$

where the limits of integration are from the maximum energy for inelastic events to the energy at the cutting point. Values of f obtained this way are listed in Tables II and III. The stated error allows for a 1-MeV uncertainty in the cutting-point energy, but does not allow for errors in the theory. It can be seen that the values of f found by the two methods generally agree within the stated errors.

4. Values of P_1P_3

$P_{3\text{ el}}$ is the analyzing power of the third scatterer for the protons scattered elastically from the deuterium target, and $P_{3\text{ in}}$ is the analyzing power at the average energy of inelastic events falling above the cutting point. Values of $P_1P_{3\text{ el}}$ and $P_1P_{3\text{ in}}$ were taken from

[7] Wilmot Hess, Rev. Mod. Phys. **30**, 368 (1958).
[8] J. I. Friedman, H. W. Kendall, and P. A. Gram, Phys. Rev. **120**, 992 (1960).
[9] G. Breit, M. H. Hull, Jr., K. E. Lassila, and K. D. Pyatt, Jr., Phys. Rev. **120**, 2227 (1960); M. H. Hull, Jr., K. E. Lassila, H. M. Ruppel, F. A. McDonald, and G. Breit, *ibid.* **122**, 1606 (1961); and private communications.
[10] S. Hee and E. H. Thorndike (to be published).
[11] A. K. Kerman, H. McManus, and R. M. Thaler, Ann. Phys. (N. Y.) **8**, 551 (1959).

values of P_1P_3 measured as a function of third scattering energy by Thorndike *et al.*[4] An error of 10% of P_1P_3 was added to the statistical error on P_1P_3 to allow for the uncertainty in the value of P_1. An error of 0.005 was also added, corresponding to an uncertainty of 1 MeV in the third scattering energy. Values of $P_1P_{3\,\mathrm{el}}$ are listed in Table V. The ratio $P_1P_{3\,\mathrm{in}}/P_1P_{3\,\mathrm{el}}$ lies between 0.891 and 0.914 for all angles of the R measurement, and between 0.898 and 0.943 for all angles of the A measurement.

IV. RESULTS

The values of R_{pd} are listed in Table VI. Also listed are the errors on R_{pd} due to the uncertainties in ϵ, $P_1P_{3\,\mathrm{el}}$, f, and R_{in}, and a quadratic combination of these four errors intended as the over-all error on R_{pd}. Table VII contains similar information about A_{pd}.

The error on R_{pd} from the error on $P_1P_{3\,\mathrm{el}}$ is small at all angles. That from the uncertainty in f is important only at 20°, where R_{pd} and R_{in} differ greatly. That from the uncertainty in R_{in} is important at small angles, out to 30°, but small beyond there. The error in ϵ dominates at 25°, 35°, and 40°, and is important at all angles.

TABLE V. Values of $P_1P_{3\,\mathrm{el}}$.

θ_2(lab)	R measurement	A measurement
20°	0.272±0.030	−0.261±0.028
25°	0.250±0.027	−0.242±0.026
30°	0.225±0.024	−0.215±0.025
35°	0.197±0.023	−0.186±0.022
40°	0.165±0.018	···

Note, however, that this error is not due to counting statistics alone; the error from possible gain shifts contributes materially, as shown in Table I. Thus, to reduce error on R_{pd} significantly, an improvement of method is required.

The error on A_{pd} from the uncertainty in f is also important only at 20° where A_{pd} and A_{in} differ considerably. That from the uncertainty in A_{in} is important out to 30°, but again small at 35°. The error in $P_1P_{3\,\mathrm{el}}$ contributes more importantly at 20° and 25°, but again the largest contribution at all angles is made by the error in ϵ.

The mean laboratory scattering energy was 140 MeV for the R measurements, and was 137.5 MeV for the A measurements. The rms spread in energy was ±3 MeV. The angular resolution of the second scattering angle varied from ±1.4° at 20° to ±1.6° at 40°.

V. COMPARISON WITH IMPULSE APPROXIMATION PREDICTIONS

The analysis of proton-deuteron elastic scattering data has been discussed by several authors, all of whom make the same basic approximations collectively referred to as the impulse approximation. Kerman,

TABLE VI. Final values of R_{pd}, with errors to R_{pd} from different sources.

θ_2(lab)	R_{pd}	Errors to R_{pd} from $\Delta\epsilon$[a]	from $\Delta(P_1P_3)$	from Δf	from ΔR_{in}	Combined error on R_{pd}
20°	+0.404	0.061	0.030	0.057	0.048	0.101
25°	+0.180	0.089	0.011	0.032	0.044	0.105
30°	+0.064	0.055	0.001	0.020	0.061	0.085
35°	−0.096	0.087	0.015	0.008	0.026	0.092
40°	+0.153	0.153	0.017	0.016	0.019	0.156

[a] $\Delta\epsilon$ is the quadratic combination of both errors to ϵ listed in Table I.

McManus, and Thaler[11] develop a theory applicable to proton-nucleus scattering in general, and discuss the above-mentioned approximations in detail. They give expressions for the cross section and polarization for p-d elastic scattering, as do Postma and Wilson,[3] and Castillejo and Singh.[12] The last authors also give expressions for the triple scattering parameters.[13]

Here we will outline the development briefly, but not attempt to justify it. The scattering matrix for scattering of an incident proton (0) by a deuteron made up of a proton (1) and a neutron (2) is written:

$$M_{pd}=F(q)\Lambda_t(1,2)[M_{np}(0,2)+M_{pp}(0,1)]\Lambda_t(1,2)\,. \quad (10)$$

$\Lambda_t(1,2)=\frac{3}{4}+\frac{1}{4}\boldsymbol{\sigma}_1\cdot\boldsymbol{\sigma}_2$ is the triplet projection operator, and restricts the initial and final states of particle 1 and 2 to triplet states, as required for elastic scattering. $M_{np}(0,2)$ and $M_{pp}(0,1)$ are the two nucleon scattering matrices for n-p and p-p scattering, which can be written

$$M_x(i,j)=A_x+B_x(\boldsymbol{\sigma}_i\cdot\mathbf{n})(\boldsymbol{\sigma}_j\cdot\mathbf{n})+C_x(\boldsymbol{\sigma}_i\cdot\mathbf{n}+\boldsymbol{\sigma}_j\cdot\mathbf{n}) +E_x(\boldsymbol{\sigma}_i\cdot\mathbf{q})(\boldsymbol{\sigma}_j\cdot\mathbf{q})+F_x(\boldsymbol{\sigma}_i\cdot\mathbf{p})(\boldsymbol{\sigma}_j\cdot\mathbf{p})\,. \quad (11)$$

These we evaluated at the energy of the incident proton and the momentum transfer of the scattering event.

$F(q)$ is the form factor of the deuteron (neglecting the finite sizes of the neutron and proton, which are included in M_{np} and M_{pp}). The unit vectors $\mathbf{n}$, $\mathbf{p}$, $\mathbf{q}$ are the conventional ones, i.e., $\mathbf{n}$ is the normal to the scattering plane, $\mathbf{q}$ is the direction of the momentum transfer, and $\mathbf{p}$ is picked so $\mathbf{n}$, $\mathbf{p}$, $\mathbf{q}$, in that order, form a right-handed triad.

TABLE VII. Final values of A_{pd}, with errors to A_{pd} from different sources.

θ_2(lab)	A_{pd}	Errors to A_{pd} from $\Delta\epsilon$[a]	from $\Delta(P_1P_3)$	from Δf	from ΔA_{in}	Combined error on A_{pd}
20°	−0.377	0.067	0.047	0.030	0.046	0.099
25°	−0.301	0.051	0.040	0.022	0.046	0.082
30°	−0.038	0.069	0.006	0.0003	0.029	0.075
35°	+0.191	0.065	0.025	0.013	0.020	0.074

[a] $\Delta\epsilon$ is the quadratic combination of both errors to ϵ listed in Table I.

[12] L. Castillejo and L. S. Singh, Nuovo Cimento **11**, 131 (1959).
[13] L. Castillejo and L. S. Singh, Nuovo Cimento **11**, 136 (1959). There is a typographical error in their expression for Γ_2 which should be the same as the $-Z$ of our Table VIII.

TABLE VIII. Expressions for p-d elastic scattering parameters in impulse approximation.

$$\Sigma_t = |A|^2+|C|^2+\tfrac{2}{3}(|B|^2+|C|^2+|E|^2+|F|^2)$$
$$\Sigma_t P = 2\,\mathrm{Re}[C^*(A+\tfrac{2}{3}B)]$$
$$\Sigma_t(1-D) = \tfrac{4}{3}(|E|^2+|F|^2)$$
$$\Sigma_t X = |A|^2-\tfrac{2}{3}|B|^2-\tfrac{1}{3}|C|^2$$
$$\Sigma_t Y = \tfrac{2}{3}(|E|^2-|F|^2)$$
$$\Sigma_t Z = 2\,\mathrm{Im}[C^*(A-\tfrac{2}{3}B)]$$
$$\sigma_{\mathrm{lab}} = \Omega(\theta_{\mathrm{lab}})F^2(q)\Sigma_t$$
$$R = X\cos\theta_{\mathrm{lab}}+Y\cos(\theta_{\mathrm{lab}}-2\alpha)+Z\sin\theta_{\mathrm{lab}}$$
$$A = -X\sin\theta_{\mathrm{lab}}-Y\sin(\theta_{\mathrm{lab}}-2\alpha)+Z\cos\theta_{\mathrm{lab}}$$
$$R' = X\sin\theta_{\mathrm{lab}}-Y\sin(\theta_{\mathrm{lab}}-2\alpha)-Z\cos\theta_{\mathrm{lab}}$$
$$A' = X\cos\theta_{\mathrm{lab}}-Y\cos(\theta_{\mathrm{lab}}-2\alpha)+Z\sin\theta_{\mathrm{lab}}$$
$$\Omega(\theta) = \frac{2(1+\gamma)}{\cos^3\theta}\left(1+\frac{\gamma+1}{2}\tan^2\theta\right)^{-2}$$
$$\alpha = \theta_{\mathrm{lab}}(\mathrm{proton})+\phi_{\mathrm{lab}}(\mathrm{deuteron})-90^\circ$$
$$A = A_{np}+A_{pp},\ B = B_{np}+B_{pp},\ \text{etc.}$$

The formulas for experimental quantities are given in Table VIII. They differ from those of Refs. 3, 11, 12, and 13 in the following respects. Since the two-nucleon amplitudes apply to the two-nucleon center of mass, the factor of $\Omega(\theta_{\mathrm{lab}})$ is required to transform the cross sections to the laboratory system. Other treatments have neglected the angular dependence of this term. In relating triple scattering parameters R, A, R', and A' to the parameters X, Y, and Z as defined by Bethe,[14] the angle 2α appears. This is because the direction of momentum transfer $\mathbf{q}$ (i.e., the direction of the deuteron recoil) does not make an angle of 90° with the direction of the scattered proton (as it does in nucleon-nucleon scattering), but exceeds 90° by the angle α. The parameters X, Y, Z are defined with respect to the direction $\mathbf{q}$, while R, A, R', A', are defined with respect to the direction of the scattered proton. Castillejo and Singh[13] set $2\alpha=0$. These two differences between our formulas and those of Refs. 3, 11, 12, and 13 tend to zero as the scattering angle tends to zero.

We have evaluated the expressions for Σ_t, P, R, A, D, R', A', X, Y, Z given in Table VIII. We have used the proton-proton amplitudes of phase parameter solution YLAM (at 140 MeV), with the n-p amplitudes of phase parameter solution YLAN 0, 1, 2, 2M, 3, 3M (at 143 MeV) of Breit and collaborators.[9] We have also used Gammel and Thaler (GT) n-p and p-p amplitudes[11] (at 156 MeV) at some angles. Coulomb effects have been included by using p-p amplitudes which include Coulomb effects. The magnetic-moment amplitude suggested by Bethe[14] for scattering from spin-zero nuclei, and used by Postma and Wilson,[3] is not included in the p-p amplitudes, and hence is not included in our treatment.

In Fig. 6 the cross-section parameter Σ_t is plotted against the laboratory scattering angle θ_{lab}. The experimental points come from the cross-section measurements of Postma and Wilson.[3] [The form factor $F(q)$ was taken from the electron scattering data of Friedman *et al.*,[8] as corrected by them for point nucleons.] Figure 7 shows the polarization as a function of θ_{lab}. Again, the experimental points are Postma and Wilson's.[3] For clarity, we have not plotted all seven curves in any graph. Beyond 20° lab, all the YLAN curves were close to YLAN 3M, for both Σ_t and P. Missing from the inset of Fig. 6 are curves for YLAN 0, 1, 3M, and GT. The curve for YLAN 0 lies between those for 2 and 2M; that for 1 follows 3 up to 10°, then rises and joins 2; that for 3M lies between 3 and 2M. The GT curve starts with 2M, rises above 2, and then falls below 3. All curves missing from the inset of Fig. 7 lie between 3M and 2M.

The calculated curves for Σ_t agree well with experiment over the entire range shown. Between 5° and 15°, curves YLAN 2, 0, 2M, and GT fit quite well, while YLAN 3M, 3, and 1 fit less well. Wilson feels the published cross-section measurements are probably high by 8%, due to an error in measuring the beam intensity. If the experimental points are lowered by 8%, then all curves fit the data about equally well in the 5° to 15° interval. The fit in the large-angle region is not appreciably worsened.

The calculated curves for P agree well with experiment at angles between 5° and 15°, and are qualitatively right out of 45°. Between 5° and 15°, all curves except YLAN 1 fit quite well. The discrepancy at angles less than 5° is perhaps of an experimental nature, as alignment is very critical for these measurements, and the beam has subsequently been shown to wander slightly.[15] Including the previously mentioned magnetic-moment amplitude has negligible effect on the Σ_t curve, but it raises the P curves, making all but YLAN 2, 3, and 3M poor fits. (Postma and Wilson,[3] calculating with GT amplitudes, get a curve which differs markedly from

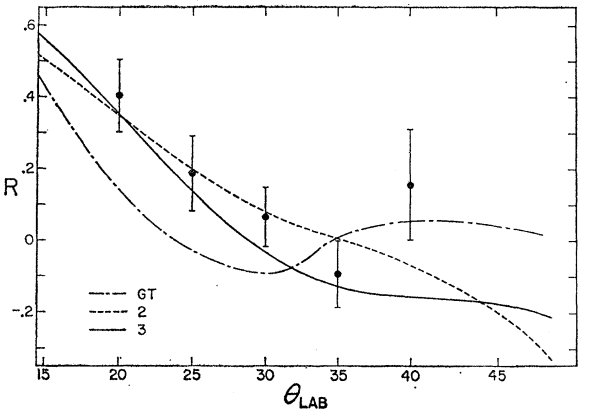

FIG. 8. R parameter versus laboratory scattering angle. The experimental points are from this article. The curves are evaluations of the expression for R given in Table VIII using the nucleon-nucleon amplitudes of Ref. 9 (YLAN 2, 3) and Ref. 11 (GT).

[14] H. A. Bethe, Ann. Phys. (N. Y.) 3, 190 (1958).

[15] D. Steinberg (private communication).

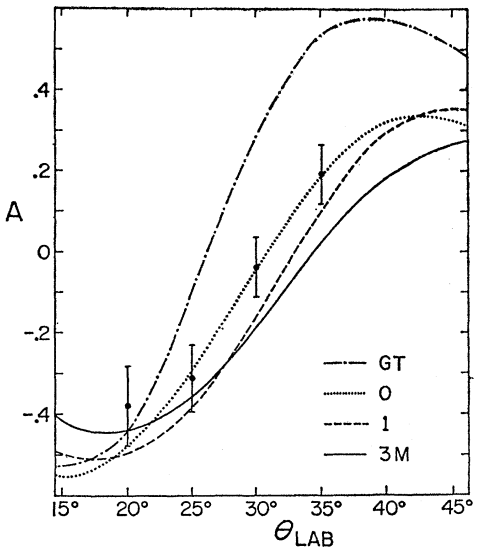

FIG. 9. A parameter versus laboratory scattering angle. The experimental points are from this article. The curves are evaluations of the expression for A given in Table VIII using the nucleon-nucleon amplitudes of Ref. 9 (YLAN 0, 1, 3M) and Ref. 11 (GT).

our GT curve in the region 5°–10°, and fits the data very poorly. We suspect a calculational error on their part. It is possible that they included a magnetic-moment amplitude four times larger than it should have been.)

If one combines the Σ_t and P results in the interval from 5° to 15°, then YLAN 2 is the best fit, and YLAN 1 is the only unacceptable solution. If one renormalizes the cross-section measurements by the suggested 8%, and combines these Σ_t and P results in the interval from 5° to 15°, YLAN 1 remains the only unacceptable solution, and YLAN 3 and 3M become the best fits.

In Figs. 8 and 9, the triple scattering parameters R and A are plotted against laboratory scattering angle θ_{lab}. Missing from Fig. 8 are curves for YLAN 0 and 2M, which lie close to 2, and YLAN 1 and 3M, which lie close to 3. Missing from Fig. 9 are curves for YLAN 2 and 2M, which lie close to 0, and YLAN 3, which lies about 0.06 below 3M.

The discrepancy between the Gammel-Thaler curve and the R measurements is, at least in part, due to the incorrect energy of the GT curve (156 MeV, rather than 140 MeV). The discrepancy between the GT curve and the A measurements is probably due to faulty amplitudes; the same discrepancy is present in the n-p measurements.

All of the YLAN curves fit the R measurements adequately. At 20° and 25° the A measurements are satisfactorily fitted by all curves, but curves 3 and 3M are low at larger angles.

VI. SUMMARY AND CONCLUSIONS

We have described an experiment measuring the p-d elastic triple scattering parameters R and A. The elastic events were identified by energy analysis of the triple scattered protons. The results are given in Tables VI and VII. Without an improvement in the method of separating elastic events from inelastic events, or without increased knowledge about the inelastic scattering, the accuracy of these results cannot be significantly improved.

The standard impulse approximation theory of p-d elastic scattering is outlined. Formulas relating the scattering parameters to nucleon-nucleon scattering amplitudes are given in Table VIII. Curves of the scattering parameters Σ, P, R, and A were calculated with the nucleon-nucleon amplitudes of the Yale group,[9] and with the Gammel-Thaler amplitudes.[11]

The GT amplitudes do not fit the p-d elastic (or the free n-p) A measurements. Yale solutions 0, 2, and 2M do not correctly describe the n-p A results. Solution 1 does not correctly describe the p-d elastic Σ and P results in the 5° to 15° interval, where the theory should be valid.

If we assume that solutions 3 and 3M are close approximations to the truth, then we may make some statements about the validity of the impulse approximation theory: (1) The theory correctly describes the experimental results out to a laboratory angle of 35° (the largest angle where Σ, P, R, and A measurements exist) with the following qualifications: The curve for P is somewhat low at 20° and 25°; that for A is somewhat low at 30° and 35°. (2). The theoretical predictions clearly deviate from the experimental results beyond 45°.

VII. ACKNOWLEDGMENTS

This experiment was a part of the nucleon-nucleon scattering program directed by Professor Richard Wilson. His support, advice, and encouragement are gratefully acknowledged. We are indebted to Professor Gregory Breit for supplying us with nucleon-nucleon amplitudes and to Dr. A. Cromer for performing the calculations from which we obtained our corrections for inelastic contamination. W. Shlaer and R. Koch assisted us in performing the experiment. Miss N. Hubbard and Miss A. Bailey reduced a large part of the data. P. Koehler helped with the impulse approximation calculations.

We wish to thank A. Koehler and the cyclotron crew for providing us with a relatively trouble-free cyclotron.